Astron. Astrophys. 293, 889–905 (1995)

ASTRONOMY
AND
ASTROPHYSICS

X-raying the interstellar medium: ROSAT observations of dust scattering halos

P. Predehl and J.H.M.M. Schmitt[1]

[1] Max-Planck-Institut für extraterrestrische Physik, D-85740 Garching bei München, Germany

Received 17 May 1994 / Accepted 2 July 1994

Abstract. We have studied X-ray halos around 25 point sources and four supernova remnants using ROSAT observations. All sources were observed during the ROSAT all-sky survey, 8 point-like sources and 2 supernovae remnants have been studied additionally using ROSAT pointed observations. The shapes of the X-ray halos were fitted with commonly used dust models (e.g., the Mathis-Rumpl-Nordsiek grain size distribution), resulting in a determination of the fractional halo intensity, which in turn can be converted into a dust column density. From the simultaneously obtained X-ray spectra, the cold gas absorption and hence an equivalent hydrogen column was determined. A surprisingly good correlation exists between the simultaneously measured dust and hydrogen column densities, indicating that gas and dust must be to a large extent cospatial. For the X-ray sources with known optical counterparts, the visual extinction correlates well with the X-ray derived dust scattering optical depth τ_{sca}: $\tau_{sca} = 0.087 \times A_v(mag) \times E(keV)^{-2}$ and $N_H[cm^{-2}/A_v] = 1.79 \times 10^{21}$. The strong correlation between both quantities indicates that, with only few exceptions, intrinsic absorption by the X-ray source itself does not affect the derived absorption column densities. This method offers also the interesting possibility of verifying the optical identification of an X-ray source by using an X-ray property itself. In particular we find that for Cas A the optical extinction and the derived X-ray scattering are on the regression line but are too low for the observed absorption. Since Cas A's supernova was not observed optically, this supernova event must have been obscured by a local dust cloud. Finally, we have found a high degree of azimuthal symmetry in all the dust scattering halos of our sample, indicating, that the majority of dust grains responsible for the halo formation cannot be highly clumped in clouds.

Key words: interstellar medium: dust – ISM: Cas A – X-rays: ISM

Send offprint requests to: P. Predehl, MPE address

1. Introduction

At optical and UV wavelengths our view of the structure of the Galaxy is severely limited by interstellar medium (ISM) absorption; at radio, infrared and X-ray wavelengths (above energies of 1 keV), however, the interstellar medium becomes sufficiently transparent to allow direct observations of a significant fraction of the Galaxy. Specifically, at soft X-ray energies between 0.1 and 2.4 keV, i.e., the ROSAT band pass, the absorption cross section of the interstellar medium changes by more than three orders of magnitude, and therefore ROSAT X-ray observations are excellently suited for probing the absorption of the interstellar medium towards distant galactic X-ray sources. Assuming a given set of element abundances, the absorption column density (usually expressed as an equivalent hydrogen column density) along a given line of sight can be measured. In this context it is worthwhile noting that the X-ray absorption (at least at energies above 0.5 keV) is primarily produced by heavier elements, mostly by oxygen and iron (Morrison & McCammon 1983); further, at these energies the absorption cross sections exclusively arise from K or L shell absorption, and therefore the absorption at X-ray wavelengths is independent from the physical or chemical constitution of the absorbing matter. This situation must be contrasted with the case of optical extinction which arises primarily from scattering (rather than genuine absorption) off grains of dust (i.e., quite complex aggregates of atoms).

Naturally, dust grains also affect the propagation of X-rays in the interstellar medium. The interaction of X-rays with cosmic dust grains leads not only to mere absorption but also to scattering, which is strongly biased into forward direction. Therefore, X-ray sources behind sufficiently dense dust clouds are expected to be surrounded by halos of faint and diffuse X-ray emission. As a consequence, X-ray observations offer an unique advantage over observations at all other wavelength ranges: With one single measurement one can determine, first, from the observed X-ray cutoff the total extinction (which is mostly due to photoelectric absorption) along the direct line of sight towards a given X-ray source, and second, from the surrounding diffuse X-ray halo the total scattering (which is exclusively due to dust grains).

Since the dust grains are also made from heavy elements, the correlation between the simultaneously measured effects of X-ray absorption and X-ray scattering should depend on the depletion of heavy elements in dust grains in the interstellar medium.

Overbeck (1965) was the first to point out the existence of dust scattering halos and their use as a powerful diagnostic tool. Further studies by Hayakawa (1970), Martin & Sciama (1970), and Martin (1970) developed a worked-out theory of the physics of X-ray scattering, and provided a detailed description of the observational signatures of X-ray scattering halos. While most of the early papers on scattering halos were of rather theoretical nature, the first detection of an X-ray halo around GX 339-4 was published by Rolf (1983), using the *Einstein Observatory*. Catura (1983) reported the detection of X-ray halos around several bright, low galactic latitude X-ray sources, and Mauche & Gorenstein (1986) showed that the shape and strength of the halos as derived from their *Einstein Observatory* measurements were consistent with common grain models, e.g., the one established by Mathis et al. (1977, MRN); the same authors also analysed halos around supernova remnants (Mauche & Gorenstein 1989).

A new era in the observational study of dust scattering halos began in 1990 with the launch of ROSAT (Trümper 1983). While all previous studies of dust scattering halos relied on a careful subtraction of an instrumental halo (caused by scattering off the X-ray optics) from the observed brightness distribution, the superb performance of the ROSAT X-ray telescope (which is characterized by an extremely low level of mirror scattering) allows, for the first time, a direct mapping of X-ray halos around many of the brighter galactic bulge sources. This was proven by Predehl et al. (1992) in the first lunar occultation measurement of a dust scattering halo with an imaging telescope; the X-ray halo around GX5-1 was directly visible while the compact X-ray source was actually behind the lunar disk. In a pilot study of the bright point source GX 339-4, Predehl et al. (1991) demonstrated how to use the ROSAT all-sky survey data for the investigation of X-ray halos. The purpose of this paper is to present a systematic study of halos around 25 point sources detected in the ROSAT all-sky survey as well as around four bright supernova remnants, all of which are sufficiently bright and sufficiently absorbed to carry out a sensitive halo determination. This large number of sources represents a complete sample of highly absorbed bright galactic sources with count rates down to ≈ 5 cts s^{-1}; a reliable determination of X-ray halos around sources fainter than ≈ 5 cts s^{-1}requires higher sensitivity than typically available in ROSAT all-sky survey data. The present paper focuses on the observed properties of dust scattering halos; as to the theory of X-ray scattering on interstellar grains, we refer to the papers by Mauche & Gorenstein (1986), Mathis & Lee (1991). Further, a companion paper (Predehl & Klose 1994) discusses the limitations of current analyses of observed dust scattering halos and the ensuing consequences for our theoretical understanding.

Our paper is structured as follows: In Sect. 2, we describe our X-ray observations and provide a detailed account of our data analysis procedures. In Sect. 3 we discuss the results, e.g., the correlations between X-ray scattering quantities and visual extinction and between the scattering depth and the interstellar absorption, and the lack of any observable azimuthal asymmetries in the observed two-dimensional brightness distributions, and finally, our conclusions are presented in Sect. 4.

2. Observations and data reduction

All observations reported in this paper have been carried out with the Position Sensitive Proportional Counter (PSPC) on board the ROSAT satellite; this detector is sensitive to X-rays in the (0.1 - 2.4) keV energy band and has been described in detail by Pfeffermann et al. (1987). All 29 sources discussed in this paper have been detected during the ROSAT all-sky survey (Voges 1992); 6 sources, (GX 17+2, GX 9+1, GX 5-1, 4U 1755-338, 4U 1705-44, 4U 1543-47) and two supernova remnants (Tycho and Kepler) were additionally observed in the ROSAT pointing program. In table 1 we present a list of all our program sources (column 1), together with the observation mode (survey or pointing, column 2), as well their position in equatorial and galactic coordinates (columns 3 to 6). Columns 7 and 8 contain the (net) observation time and the number of counts contained in the source, which allows an assessment of the statistical accuracy of our results. As can be seen from Table 1, the typical observation times for a pointed observation of our sample range between 2500 and 6000 sec, while for the all-sky survey, typical exposure times are less than 100 sec, distributed in about 10 sec pieces during the characteristic two day survey visibility interval. However, the X-ray sources in Cygnus and the Large Magellanic Cloud (LMC) regions were exposed longer because of their location at high ecliptic latitudes. These rather low numbers result from a restriction of the field of view (see below). Since we have also limited the spectral range, the number of counts (last column) is less than the total number of events received from the source. Therefore, both numbers cannot be used to calculate count rates.

2.1. Spectral fits

We performed spectral fits to our data using the EXSAS software system developed at MPE. Since all of our sources appear extended (because of the presence of an X-ray halo), one must decide whether the photon extraction for a spectral fit should apply to the central source, the X-ray halo or both. Since we are only interested in the interstellar absorption value which is not expected to significantly differ for the central source and the halo, we have chosen a radius of 500 arcsec. In order to obtain a quantative interpretation of our PSPC pulse height spectra, we applied three different spectral models, i.e., a power law, a thermal bremsstrahlung, and a black body model, to each source (except for the supernova remnant sources). Since all the sources show a low energy cutoff in their PSPC pulse height spectra (otherwise one would of course not expect to detect any X-ray halo !), all the spectral models must also include cold gas absorption, which was modelled using the absorption cross sections given by Morrison & McCammon (1983). A summary of our spectral

Table 1. List of sources with the mode of observation (pointing or survey), their positions in equatorial and galactic coordinates, the (net) observing time, and the number of events which have been taken for the analysis.

Source	mode	R.A. [2000]	Dec. [2000]	l^{II}	b^{II}	t_{obs}	counts
Cyg X-1	S	$19^h58^m23^s$	$+35^d10'48''$	71.3^d	3.1^d	111	5125
Cyg X-2	S	$21^h44^m40^s$	$+38^d19'14''$	87.3^d	-11.3^d	128	21733
Cyg X-3	S	$20^h32^m12^s$	$+40^d56'30''$	79.8^d	0.7^d	110	662
Ser X-1	S	$18^h39^m58^s$	$+5^d02'08''$	36.1^d	4.9^d	63	3768
GX 17+2	P	$18^h39^m58^s$	$-14^d02'07''$	16.4^d	1.3^d	4385	113418
GX 13+1	S	$18^h14^m32^s$	$-17^d09'32''$	13.5^d	0.1^d	47	270
GX 9+9	S	$17^h31^m42^s$	$-16^d58'00''$	8.5^d	9.0^d	77	6558
GX 9+1	P	$18^h01^m30^s$	$-20^d31'37''$	9.1^d	1.2^d	2027	62199
GX 5-1	P	$18^h01^m08^s$	$-25^d04'31''$	5.1^d	-1.0^d	4281	130801
GX 3+1	P	$17^h47^m56^s$	$-26^d33'40''$	2.3^d	0.8^d	5003	74167
EQ 1731-260	S	$17^h34^m14^s$	$-26^d06'08''$	0.7^d	3.4^d	55	744
GS 1734-275	S	$17^h36^m01^s$	$-27^d26'08''$	0.8^d	1.6^d	66	2429
GX 349+2	S	$17^h05^m42^s$	$-36^d26'13''$	-10.9^d	2.8^d	45	3292
4U 1820-30	S	$18^h23^m40^s$	$-30^d21'51''$	2.8^d	-7.9^d	56	5127
4U 1755-338	P	$17^h58^m41^s$	$-33^d48'28''$	-2.8^d	-4.9^d	1888	165485
4U 1705-44	P	$17^h08^m54^s$	$-44^d06'10''$	-16.7^d	-2.4^d	5248	107966
GX 339-4	S	$17^h02^m46^s$	$-48^d48'37''$	-21.1^d	-4.3^d	56	11793
V801 Ara	S	$16^h40^m53^s$	$-53^d46'15''$	-27.1^d	-4.8^d	92	3385
4U 1556-60	S	$16^h01^m03^s$	$-60^d44'48''$	-35.9^d	-5.9^d	83	444
Cir X-1	S	$15^h20^m39^s$	$-57^d09'53''$	-27.9^d	0.0^d	99	7778
LMC X-1	S	$5^h39^m24^s$	$-69^d45'15''$	-79.8^d	-31.5^d	414	2673
LMC X-2	S	$5^h20^m27^s$	$-71^d58'10''$	-77.0^d	-32.7^d	192	1200
LMC X-3	S	$5^h38^m56^s$	$-64^d05'47''$	-86.4^d	-32.1^d	97	670
4U 1543-47	P	$15^h47^m08^s$	$-47^d40'19''$	-29.1^d	5.4^d	1887	1053484
PKS 2155-304	P	$21^h58^m52^s$	$-30^d13'40''$	17.7^d	-52.2	53750	348800
Cas A	S	$23^h23^m30^s$	$+58^d50'00''$	111.8^d	-2.1^d	111	1765
Tycho	P	$00^h25^m20^s$	$+64^d09'00''$	120.1^d	$+1.4^d$	25690	473672
Kepler	P	$17^h30\ ^m41^s$	$-21^d31'31''$	4.5^d	$6.8\ ^d$	32214	2068
Crab	S	$05^h34^m39^s$	$+22^d01'10''$	184.6^d	-5.8^d	83	49791

fit results is given in Table 2, where we list again the source name (column 1), quote an N_H value taken from the literature (column 3), and report the N_H values together with their statistical errors and the overall quality of the spectral fit expressed in terms of the χ^2 test statistic for the power law model (column 3 - 5), for the thermal bremsstrahlung model (column 6 - 8, and for the for the blackbody model (column 9 - 11). As can be seen from Table 2 and Fig. 2 (see below), our spectral fits give no preference for either a black body or a thermal bremsstrahlung spectrum model; some sources can be better fit by the former, others by the latter model, while in a few cases both models result in acceptable fits. Interestingly, for all our sources power law fits were always acceptable and consistent with the better fit of the other two models. This can be naturally explained by the rather narrow effective ROSAT band pass (between the low energy cutoff by absorption and the high energy cutoff by the ROSAT mirror) left over for highly absorbed sources, since over such a narrow energy range a spectrum can always be reasonably approximated by a power law. We therefore decided to use the values obtained by our power law fits in all cases. The spectra of the shell type supernova remnant Cas A has been fitted with a thermal line emission model (assuming collisional ionisation equilibrium) as derived by Raymond & Smith (1977). The spectra of Tycho & Kepler could not be fitted in a straightforward manner. Therefore we decided to rely on the literature values alone.

2.1.1. Remarks on individual sources

The purpose of this paper is not a detailed study of the properties of individual sources, rather our paper focusses on the statistical properties of a large sample of sources with simultaneously derived absorption and scattering column densities. Since by necessity all our sources are strong X-ray sources, essentially all of them were previously studied with different instruments. The purpose of this section then is to compare – for a few individual cases – our N_H values with those derived by other authors, and check to what extent these values possibly depend on the band passes of the different instruments and different source models used. Specifically, we compare our results to those of White et al. (1988), who fitted four different physically motivated models to EXOSAT data on 12 X-ray binaries, and found only marginal influence to the N_H–values, and to those of Schulz et al. (1989), who carried out spectral studies of 21 X-ray binaries, again observed with EXOSAT.

Table 2. List (all N_H values are in 10^{21} cm^{-2}). The literature values (column 2) are taken from Schulz, Hasinger, and Trümper 1989 (1) and from White, Stella, and Parmar 1988 (2) for the point sources. The two SNR–values have been taken from Becker et al. (1980) for Kepler and Hamilton et al. (1986) for Tycho. Our fits used power-law (pwl), thermal bremsstrahlung (thb), and black body (bbd) models. A thermal model (Raymond & Smith) has been used for Cas A.

Source	N_H (Lit)	N_H (pwl)	err	χ^2	N_H (thb)	err	χ^2	N_H (bbd)	err	χ^2
Cyg X-1		4.1	0.4	1.0	4.0	5.9	1.0	2.6	0.3	1.1
Cyg X-2	3[1]	2.5	0.2	1.9	2.5	0.2	2.1	0.7	0.1	2.7
Cyg X-3		33.1		1.7	40.5		1.7	0	24.	5.4
Ser X-1		5.1	0.5	1.2	5.0	9.0	1.2	3.0	0.3	1.2
GX 17+2	19[1], 21[2]	20.6	3.3	1.2	23.4	17.	1.5	17.9	1.2	1.3
GX 13+1	29[1]	27.9	66.	1.1	31.7	33.	1.0	0	28.	3.2
GX 9+9	2[1]	2.6	0.3	1.5	2.5	3.0	1.5	0.8	0.2	1.5
GX 9+1	15[2], 18[1]	15.6	4.6	1.0	18.7	57.	1.3	13.6	1.2	1.0
GX 5-1	33[1]	30.8	6.8	1.2	34.8	28.	1.5	27.8	2.2	1.1
GX 3+1	12[1], 16[2]	17.0	2.3	1.2	17.8	48.	1.2	14.2	0.9	1.2
EQ 1731-260		12.6	2.1	1.3	12.8	32.	1.3	10.0	1.9	1.3
GS 1734-275		11.6	1.4	1.2	10.8	4.4	1.2	8.3	0.2	1.2
GX 349+2	8[2]	9.6	0.7	1.8	37.8	2.5		7.1	0.5	1.7
4U 1820-30		2.4	0.4	1.2	2.1	0.5	1.2	3.6	0.2	1.2
4U 1755-338		3.8	0.2	1.1	3.7	1.6	1.0	1.8	0.1	1.5
4U 1705-44		14.7	1.8	1.2	16.3	34.	1.4	12.3	0.7	1.2
GX 339-4		6.7	0.3	1.5	5.9	0.6	1.5	3.8	0.1	1.5
V801 Ara		3.6	0.5	1.0	3.5	2.7	1.0	0.3	1.1	1.1
4U 1556-60		3.2	1.4	1.3	3.2	2.1	1.4	1.5	0.9	1.3
Cir X-1		22.3	6.5	1.6	24.1	38.4	2.6	19.9	2.7	1.6
LMC X-1		9.4	0.8	1.1	16.0	1.0	3.5	5.9	0.5	1.1
LMC X-2		1.1	0.5	1.1	0.9	0.3	1.1	0.0	0.3	1.3
LMC X-3		1.1	0.4	1.0	0.7	0.1	1.0	0.0	0.3	1.5
4U 1543-47		4.9	0.1	1.0						
PKS 2155-304		0.2	0.0	1.8						
Cas A		18.3	0.37	1.35						
Tycho	4.0									
Kepler	6.0									
Crab		2.9	0.1	2.8	2.06	0.1	3.0	3.4	0.05	4.6

Except for the supernova remnant sources, all the sources producing X-ray halos are intrinsically time variable. To what extent intensity variations in these sources are accompanied by spectral variations is a subject of current research. Clearly, the amount of interstellar absorption should never change, however, the deduced values for N_H may depend on the assumed spectral models; in addition, some sources may be intrinsically absorbed. In Table 2 we provide a list of published N_H values for our sample sources; the values were taken from only two papers (White et al. 1988; Schulz et al. 1989) because we are interested only in the reliability of our own data but not in a general analysis of spectral models. Inspection of Table 2 shows a very good correlation between published N_H values and those derived by us.

Finally, according to to Gorenstein (1975), Cyg X-1 appears to have significantly less absorption in its X-ray spectrum ($N_H \approx 1 - 1.5 \times 10^{21} cm^{-2}$) than the extinction of its optical counterpart would indicate. Its spectrum shows a soft component in excess of the spectral function which describes its spectrum above 2 keV. The lightcurve of Cyg X-1 exhibits dips during which an excess flux below 4 keV (Kitamoto et al. 1989) can be attributed at least partially to scattered X-rays; these authors found the interstellar absorption to be $N_H = 2 \times 10^{22} cm^{-2}$. *ROSAT* has observed Cyg X-1 during the ROSAT all-sky survey in more than 30 individual scans. Intensity variations are recognized but averaged over the observation period of several days.

In summary, the fact that our survey observations result in time-averaged flux values for all our sources together with the fact that the effective *ROSAT* energy band is restricted to a small region around the the absorption "edge" caused by the interstellar medium (but not by intrinsic source absorption), leads to the conclusion that our spectral modelling is in fact sufficiently accurate for the determination of ISM N_H; this view is supported by the excellent agreement between our N_H values with those reported in literature.

2.2. *Scattering halo determination*

The derivation of the X-ray halo from the X-ray surface brightness distribution requires a knowledge of the instrument point response function (PRF), a proper determination of the background brightness, and – possibly – the subtraction of the con-

tribution of serendipitous point-like sources from the measured radial intensity distribution profile. The most general way of determining an X-ray halo is to subtract a model point response function (PRF) from a measured radial surface brightness distribution; the model PRF can be derived either from ground measurements or from in-orbit measurements of sources not suspected to be surrounded by X-ray halos. This method is not quite exact since – strictly speaking – the observed brightness distribution is the convolution (and not the sum) of the combined contributions of central source and halo and the instrumental PRF. In practice, however, the errors are very small when compared with the errors arsing from the usual assumptions made on the scattering cross sections, the influence of the chemical composition of the grains and so forth. All these simplifications affect the grain size distribution and the spatial distribution along the line of sight, but not the total fractional halo intensity, the quantity which we are interested in primarily.

In order to assess our analysis procedures we checked our model PRF with a non-halo source; as a calibration target we used a deep on-axis PSPC observation of the the high latitude source PKS 2155-304. This observations contains more than 2×10^6 counts from the target, and yet our halo analysis procedure results in no detectable X-ray scattering halo around PKS 2155-304; this finding is in agreement with expectations because of the low column density towards PKS 2155-304. In the following we will discuss the adopted point response function for both the pointing and survey mode.

2.2.1. Point response function in pointing mode

The core of the PRF of an on-axis ROSAT PSPC observation (as is the case with all our pointed observations) is dominated by detector properties; while the X-ray telescope and uncertainties in the aspect system contribute < 5 arcsec FWHM to the PRF, the detector itself contributes ≈ 20 arcsec FWHM. Therefore, in a first approximation, the intrinsic spatial resolution of the ROSAT PSPC can be described by a Gaussian with a width of $\approx E^{-1/2}$ (Hasinger et al. 1993). Outside the central region, the Gaussian shape of the PRF is modified by focus and penetration effects caused by the detector as well as scattering off the X-ray mirror. The distance between the mirror and the detector, i.e., the focal length of the X-ray telescope (XRT), is chosen in such a way that on-axis photons with an energy of ≈ 1 keV are brought to a focus at an optimum depth within the PSPC drift region (in order to minimize the detector intrinsic Gaussion width). For photons with energies different from 1 keV, this width increases, leading to a radial shape of the outer wings of the PRF which can be modelled as a Lorentzian. At even larger radii, the radial PRF profile wings can be well described by a power law profile, caused by the microroughness of the mirror with ensuing X-ray scattering. The scattered intensity scales approximately as $I_{scat} \approx 0.03\ (E/1keV)^2$; this value of scattered intensity is very small compared to the performance of all previously flown X-ray telescopes.

Due to vignetting effects, i.e., the decreasing sensitivity of the X-ray telescope as a function of off-axis angle, the effective exposure of a source and its halo is not uniform. Special attention must therefore be devoted to the construction of a correct exposure map. A further complication arises from the fact that all contributions to the PRF as well as to the halo depend on photon energy which is only approximately measurable. In a first approximation, the correlation between incident photon energy and measured pulse height is roughly linear. Because of the only modest energy resolution of PSPC, pulse height spill-over effects can however lead to deviations from a simple linear correlation, since the actual correlation now depends on the incident photon spectrum (Mauche & Gorenstein 1986). In order to illustrate this effect, consider a hypothetical source with a flat power law energy spectrum (i.e., photon index -1) and an observed PSPC pulse height channel just above the carbon edge. At these energies the effective area of the PSPC is extremely small, and hence any event recorded in such a pulse height channel must result from spill-over. If our hypothetical X-ray source has an interstellar absorption column density of, say, $N_H = 3 \times 10^{21}\ cm^{-2}$, all photons below the carbon edge are absorbed, and therefore the mean and most probably energy of such an event is far above the nominal channel energy; if, on the other hand, our hypothetical source is observed with no absorbing column, the same pulse height event would very likely be caused by a photon below the carbon edge (simply because there are far more photons below than above the carbon edge because of the assumed spectrum). Therefore, the most likely energy of a recorded event must depend on the underlying incident photon spectrum; for a detailed description of our procedure to assign a mean energy to each pulse height channel we refer to the companion paper by Predehl & Klose (1994).

Serendipitous X-ray sources – whenever present in the halo of our sources – have been removed; the same region was then also been removed from the exposure map, leaving the resulting surface brightness distribution correct.

Unlike the procedures adopted in previous investigations (cf. Mauche & Gorenstein 1986), the background was not be taken from nearby fields or from an annulus around the source. The background of the ROSAT PSCP is almost always dominated by the diffuse X-ray background which, particularly in the Galactic Center region, can be highly structured. Furthermore, as mentioned above, the halos of some of our sources actually exceed the field of view of the ROSAT PSPC; note that this point is of course relevant only for pointed data. Therefore, the background (with values typically as low as about $10^{-4} s^{-1} arcmin^{-2}$) was taken as a free parameter of the model fit; over the measured extent of an X-ray halo, the background was of course assumed to be uniform.

2.2.2. Point response function in survey mode

All the components in the pointing PRF identified in the previous section are also present in the brightness distribution profiles of sources observed during the all-sky survey. In general, the analysis of survey data is far more difficult because the sources are scanned and thereby viewed at all possible off-axis angles. The off-axis PRF of grazing incidence ROSAT mirror is rather com-

plicated. The RMS blur-radius, defined as the radius containing 68% of all photons, increases, slowly at first and then quite rapidly for off-axis angles larger than 20 arcmin. For off-axis angles less than 40 arcmin, the off-axis PRF can be reasonably approximated by an off-axis angle dependent Gaussian; for even larger off-axis angles, the PRF can no longer be described by sufficiently simple analytical models, which is the reason why we decided to artificially restrict the telescope's field of view to the inner 40 arcminutes. Within this region, the shape of the PRF can be modelled sufficiently well by a Gaussian core broadened by an off-axis dependent term. The total PRF was calculated by constructing an off-axis exposure histogram and summing the appropriately weighted individual contributions. Finally we note that the restriction to the inner 40 arcmin also reduced the effective observation time to about 10 sec per scan.

A further remark concerning the uniformity of coverage of our sources seems appropriate. Since the PSPC high voltage had to be switched off during passages of the earth's radiation belts and the South Atlantic Anomaly, these areas are projected onto the sky as less exposed areas; especially the sources south of the Galactic Center are affected by such observing time losses, which resulted in an effective integrated exposure time of less than 100 sec for most of the sources studied in this paper. However, the great advantage of the survey observation is that the area of interest is not restricted by the telescope's field of view. Some of the brightest sources (e.g., GX 339-4, Crab) have halos which can be followed out to radii of more than one degree away from the central source.

As an example of the survey data, we show the ROSAT all-sky survey observations of GX 339-4 in detector coordinates (cf. Fig. 1). The image displayed in Fig. 1 was constructed in such a way, that all the photons received from GX 339-4 (or rather all photons received from a small region around GX 339-4) are shown as they were recorded on the scanning detector. If this source had received its full exposure, the whole detector would have been more or less uniformly illuminated with source photons; the actual photon distribution is obviously quite inhomogeneous, with exposure gaps, vignetting effects, and the sharpening of the point response near on-axis angle being immediately obvious. From Fig. 1 it is clear that the use of a mean PRF for all of our sources would have led to totally spurious results, because all of our sources have different exposure histories.

2.2.3. Instrument function for supernova remnants

The halos around the four supernova remnants have also been investigated; unlike the X-ray binaries in our sample, the central sources are extended; we decided to model the central sources (i.e., the supernova remnants) by a simple boxprofile. Clearly, this procedure leads to some inaccuracies within the inner 2 arcmin of the halo; however, it has no significant influence on the derivation of the fractional halo intensity (the quantity we are primarily interested in) since the halo contribution within the core is small (cf., Fig. 10.26 – 10.29).

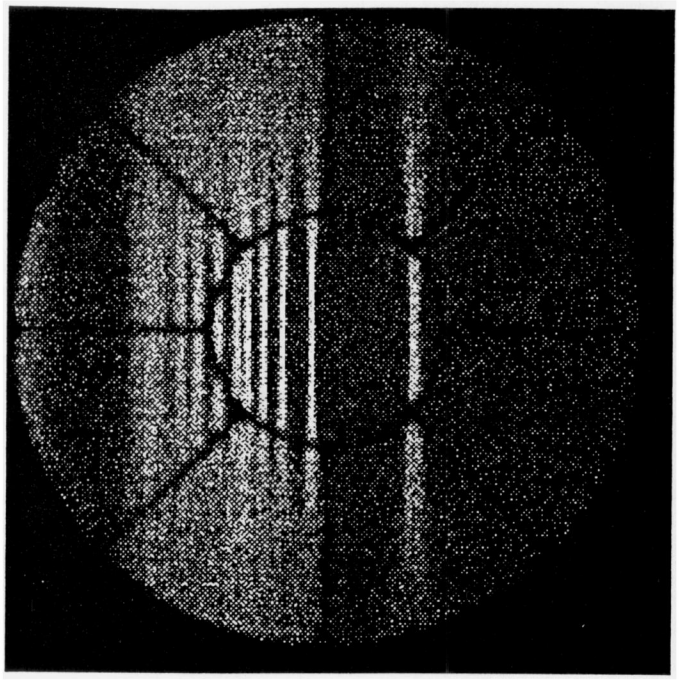

Fig. 1. Survey observation of GX 339-4 in detector coordinates. According to the survey geometry a particular source takes about 30 sec to travel through the 2^o field of view of the PSPC. The window support structure is smeared out when photons are projected onto the sky. The effects of data gaps due to South Atlantic Anomaly passages during which the detector had to be switched off as well as the effects of off-axis blurring due to the telescops's point response function can be clearly seen

2.3. *Model halos*

Our general procedure to extract halo parameters from our PSPC observations consists in fitting the measured surface brightness distribution to a model containing a central point source, a uniform background, and, of course, a theoretical halo. The PRF and the background were fitted by their normalization only, keeping energy dependence and shape fixed. For the model halo we assumed a power law grain size distribution, characterized by some slope q between given grain size limits a_{min} and a_{max}; since the halo shape does not sensitively depend on the smallest grains, we reduced the number of free parameters by setting the lower grain size limit to zero, i.e., $a_{min} = 0$. We further assumed the dust uniformly distributed along the line of sight between the source and the observer within the limits x_{min} and x_{max}, where x_{min} and x_{max} denote fractional distances towards the source, i.e., $0 \leq x_{min} < x_{max} \leq 1$. Thus, the dust model is represented by four parameters a_{max}, q, x_{min}, and x_{max}. As a scattering model, we used the usual Rayleigh-Gans theory in its Gaussian approximation (see also Mauche & Gorenstein 1986; Mathis & Lee 1991; Predehl et al. 1991). The scattered intensity measured by an observer at the angular distance Θ_{obs} is given by

$$I(\Theta_{obs}) = \text{const.} \int_{E_{min}}^{E_{max}} dE\, S(E) \int_0^{a_{max}} da\, a^{-q}$$

$$\times \int_{x_{min}}^{x_{max}} dx \; \frac{d\sigma(\Theta_{\rm scatt}, a, E, x)}{d\Omega} \; \frac{1}{(1-x)^2} \; , \qquad (1)$$

with $\Theta_{\rm obs} = (1-x)\,\Theta_{\rm scatt}$; a detailed description and justification for the use of Eq. (1) is given by Predehl & Klose (1994). In addition to already explained symbols, $S(E)$ denotes the measured spectral energy distribution of the point source in the energy band $[E_{\rm min}, E_{\rm max}]$ of the observation; a^{-q} denotes the size distribution function of the scattering particles (which are assumed to be spherical and characterized only by their radius a); and $\frac{d\sigma(\Theta_{\rm scatt},a,E,x)}{d\Omega}$ denotes the differential scattering cross section for a single dust grain; for a detailed discussion of the form of the cross section $\frac{d\sigma(\Theta_{\rm scatt},a,E,x)}{d\Omega}$ we again refer to Predehl & Klose (1994).

In Fig. 10.1 – 10.29 we show the measured X-ray surface brightness distributions (in units of PSPC cts sec^{-1} arcsec^{-2}) as a function of radius (measured in arcsec) for all our sample sources. In each plot we show the measured data points with their statistical errors (vertical lines and bars), the point response function (long dashed curve) modelling the radial intensity of the central point source, the X-ray halo (dotted curved) derived from fitting Eq. (1) to the observed brightness distribution, and the overall model distribution consisting of central point source, halo, and uniform background (solid curve); in addition, each panel contains the source name as well as the derived fractional halo intensity (in percent). As is obvious from Fig. 10, the central point source clearly dominates the surface brightness distribution in the inner 1 - 2 arcminutes; for many of our sample sources, the halo dominates at distances greater than 1 - 2 arcminutes. However, in some cases (LMC X-1, LMC X-2, LMC X-3, GX 9+9), the inferred halo surface brightness never exceeds the modelled point response. The case of LMC X-2 (cf. Fig. 10.17), for which we find essentially no detectable halo, shows our capability to model the survey point response function; the BL Lac object PKS 2155-304 has been used as calibration source for the PRF, and its halo is therefore zero by definition (cf. Fig. 10.1).

The determination of the fractional halo intensity does not sensitively depend on the dust model used (cf. Mathis & Lee 1991; Predehl & Klose 1994). Specifically, our expression (cf. Eq. 1) for the angular distribution of the scattered intensity is valid – in addition to a number of other assumptions – for single scattering only. Mathis & Lee (1991) have emphasized the importance of multiple scattering processes in the analysis of X-ray halos. We wish to point out that we use Eq. (1) only to determine the **fractional halo intensity**; the largest source of error in the fractional halo intensity determination lies in the extrapolation of the model halo into the unresolved core of the point response function where single scattering definitely dominates.

The fractional halo intensity I_{frac} can be transformed into an optical depth due to scattering using the equation (cf. Eqs. 2.12 and 2.13 in Mathis & Lee 1991)

$$I_{frac} = \frac{I_{halo}}{(I_X + I_{halo})} = (1 - e^{-\tau_{sca}}). \qquad (2)$$

Here the optical depth τ_{sca} is the product $N_{dust} \times \sigma_{dust}$, with N_{dust} denoting the total column density of grains along the line of sight and σ_{dust} the (mean) dust scattering cross section, I_X denotes the (absorbed) flux from the central source, and I_{halo} the measured (and therefore also absorbed) total halo flux.

Table 3 provides a summary of our halo determination results. For each of our sample source (specified in column 1), it contains in particular the mean energy (in column 2, defined as the energy of the peak of the observed PSPC pulse height distribution), and the fractional halo intensity in column 3. As already found by Mauche & Gorenstein (1986), no single grain size is capable of producing the observed halos. We have used the MRN-model which is based on a powerlaw grain size distribution. The derived dust parameters q and a_{max} are in columns 4 and 5; the last column contains the fitted background value. The value for the mean energy has been obtained by weighting the individual photon energies according to the energy dependence of the scattering cross section, i.e., approximately $\sim E^{-2}$. The optical depth τ_{sca} is calculated by inverting Eq. (2). This optical depth refers to the mean effective energy of the source photons considered (cf. Table 3, col. 9). In order to compare the halos measured for different sources at different mean energies, we remove the energy dependence of the optical depth by normalizing at 1 keV according to

$$\tau_{sca}(1keV) = \tau_{sca} \times E^2_{mean}. \qquad (3)$$

3. Discussion of results

The main quantities derived from our X-ray analysis for each of our sample sources are the equivalent hydrogen absorption column density N_H and the fractional halo intensity I_{frac}. We will now study the reliability of these measurements, and various correlations between our measurements and source parameters derived by other means.

3.1. N_H column densities

Since the column densities are derived from model fits, we must ask ourselves how reliable these values actually are. As is obvious from Fig. 2, there is an extremely tight correlation between the N_H values derived from rather different spectral models. A linear regression analysis results in the following expressions between the various N_H parameters (N_H is given in units of 10^{21} cm^{-2}): $N_{H,th} = N_{H,pl} \times 1.14 - 0.41$ and $N_{H,bb} = N_{H,pl} \times 0.95 - 1.70$. As can be seen from Fig. 2, blackbody fits tend to produce lower N_H values than the corresponding power law or bremsstrahlung fits; this is easily attributable to the nature of the blackbody spectra which are – for our spectral fits – rather flat or even turn over in the ROSAT band pass.

As a result of our spectral fits we conclude that, first, in the ROSAT PSPC band pass the apparent spectral shape of our sources is dominated by the strongly energy dependent transmission of the interstellar medium, and second, that the intrinsic, i.e., de-reddened, spectral shape of our sources remains essentially unconstrained. The spectral models themselves are therefore not discussed in this paper, they are - fortunately - also

Table 3. List of sources with the visual extinction A_V, the average photon energy, weighted by the scattering cross section, the exponent q of the power-law grain size distribution $n(a) \approx a^{-q}$, the upper grain size limit, and the background brightness [10^{-8} cts s^{-1} arcsec^{-2}]. The values for the visual extinction have been taken from (1) Bradt and McClintock 1983, (2) Van Paradijs 1991, (3) Garcia et al. 1992, (4) Chevalier 1989, (5) Penninx and Augusteijn 1992, and (6) Mauche and Gorenstein 1989.

Source	A_V	E_{mean}	I_{halo} (%)	q	a_{max}	bkgr
Cyg X-1	3.3[1]	1.20	11.6	3.7	0.32	7.46
Cyg X-2	1.3[1]	1.06	3.9	4.0	0.15	6.33
Cyg X-3	19.[1]	1.72	40.4	3.8	0.20	0.92
Ser X-1	1.5[1]	1.21	9.4	3.5	0.20	9.75
GX 17+2	(2.0)[1]	1.59	32.9	4.4	0.16	2.91
GX 13+1	14.[3]	1.69	33.5	3.8	0.18	7.28
GX 9+9	1.0[1]	1.08	3.6	3.5	0.22	18.3
GX 9+1	10.[2]	1.55	24.3	4.4	0.16	4.28
GX 5-1		1.71	25.4	4.2	0.20	7.44
GX 3+1	11.[2]	1.54	26.3	4.1	0.19	6.45
EQ 1731-260	9.6[2]	1.44	22.8	3.5	0.13	6.38
GS 1734-275		1.35	18.4	3.6	0.15	21.6
GX 349+2	5.0[5]	1.39	18.7	4.2	0.15	4.08
4U 1820-30	0.8[1]	1.05	3.2	3.2	0.15	24.2
4U 1755-338	1.0[1]	1.18	7.4	4.8	0.20	21.3
4U 1705-44		1.53	27.9	4.1	0.15	4.98
GX 339-4	3.5[1]	1.2	9.6	4.4	0.17	3.00
V801 Ara	1.0[1]	1.16	4.6	4.0	0.20	16.8
4U 1556-60	1.9	1.17	7.1	4.2	0.05	11.9
Cir X-1	11.[1]	1.59	29.2	4.0	0.18	1.03
LMC X-1	0.8[2]	1.26	2.1	3.8	0.18	24.9
LMC X-2	0.8[2]	1.01	0.2	3.4	0.12	5.38
LMC X-3	0.8[2]	0.91	0.6	3.8	0.18	9.16
4U 1543-47	2.2[4]	1.12	8.0	2.5	0.15	6.40
PKS 2155-304		0.86	0.0	—	—	3.75
Cas A	5[6]	1.24	16.1	4.0	0.18	1.26
Tycho	2.3[6]	0.93	18.0	4.3	0.20	8.71
Kepler	3.5[6]	0.91	16.8	4.4	0.16	4.08
Crab	1.6[6]	1.02	9.1	4.1	0.18	3.37

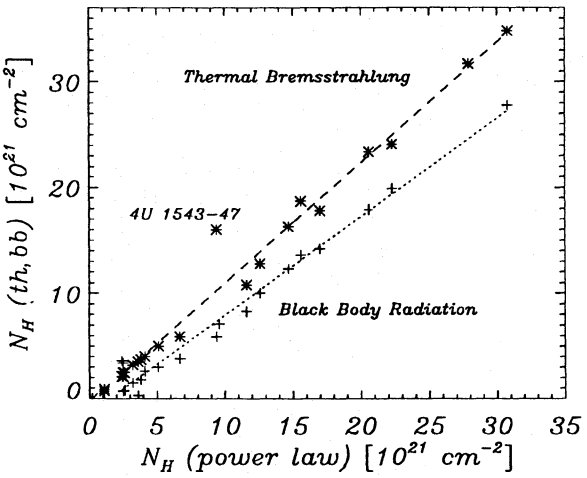

Fig. 2. The spectral model dependence of N_H - values: N_H derived from assuming thermal bremsstrahlung (stars and fitted dashed line), or black body models (crosses, dotted line), respectively, vs. power law models. This plot shows the accuracy with which the absorbing column density can be determined

not needed for our halo analysis; the required N_H values can however be determined well and are to a large extent model-independent.

3.2. The relation between X-ray absorption and optical extinction

As a side product of our X-ray halo studies, we can take a new look at the relationship between X-ray absorption (measured through the absorption column densities in our spectral fits) and the optical extinction (characterized through A_v); in Table 3 we list the A_v, published for our sample sources. The corresponding values are plotted in Fig. 3 together with the absorption column densities derived from our PSPC spectra. The dotted curve is a regression line, numerically given by $A_v = 0.56\ N_H[10^{21}\ cm^{-2}] + 0.23$, from a linear fit to the data; the outliers, i.e., LMC X-1, GX17+2, and Cas A were not included in the regression analysis. Garcia et al. (1992) have determined the visual extinction for GX 13+1. They found $10.2 \leq A_V \leq 14$. From a comparison with the X-ray halo as measured with the Einstein Observatory, they suggested that the

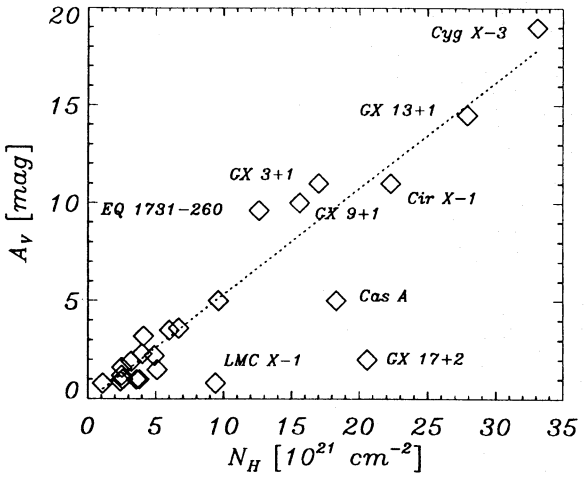

Fig. 3. Visual extinction vs. equivalent hydrogen column density. The fit (dotted line) does not contain GX 17+2 and LMC X-1. It yields $N_H = 1.79 \pm 0.03\ A_V[mag] \times 10^{21}[cm^{-2}]$

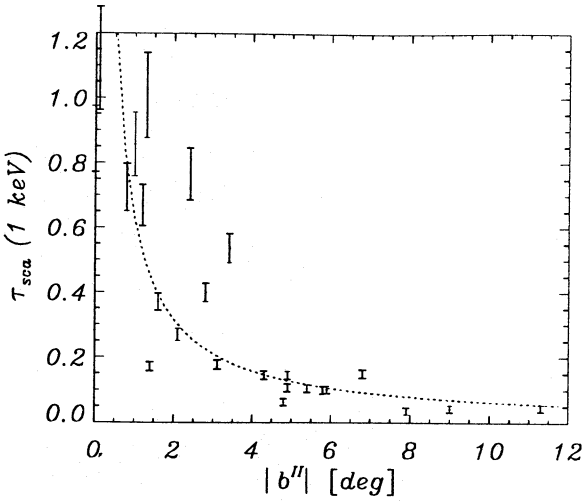

Fig. 4. The dependency of the optical depth in scattering on the galactic latitude. The dotted line ($\approx$ 0.1 / $sin(b^{II})$ [kpc]) is simply fitted by eye

lower value is more likely. Using the same argument, $A_V = 14$ fits better to our data for the X-ray halo (see below) as well as the absorption (Fig. 3). As far as LMC X-1 is concerned, such a significant deviation from the correlation between A_V (=dust) and N_H (= cold gas + dust) requires a dust to gas ratio far from the canonical value. This can be produced, for instance, by absorption in the vicinity of the X-ray source, and we suspect that the nebula discovered by Bianchi & Pakull (1985) is a good candidate for producing the required additional absorption. The discrepancy for GX 17+2 can be ascribed to an incorrect optical identification; as already noted by Naylor et al. (1991), the optical counterpart of GX 17+2 should have an extinction of $A_v \sim 11$ in order to be consistent with both the X-ray absorption and X-ray scattering measurements, a conclusion which is fully supported also by our results (cf. Fig. 6).

An earlier version of this correlation (cf. Fig. 1 in Gorenstein 1975) resulted in a slightly different slope of the correlation line (0.45 instead of our 0.56); however, given that both Gorenstein's (1975) and our N_H determinations suffer from systematic uncertainties, we feel that no weight should be attached to this discrepancy. We further note in passing that our zero point offset corresponds to a column density of $2.3 \times 10^{20}\ cm^{-2}$, which is much less than the smallest column density of any of our sample sources. Since Gorenstein's (1975) N_H-values were derived from supernova remnants only, i.e., from X-ray sources **without** any plausible intrinsic absorption, we interpret the good agreement between our and Gorenstein's (1975) A_v vs. N_H correlation as evidence that all our sample sources are also free of intrinsic absorption. Converting A_v to E_{B-V} using the canonical relation $A_v = 3\ E_{B-V}$, we find $N_H = 5.3 \times 10^{21}\ cm^{-2} E_{B-V}$, which agrees very well with the correlation between N_H and E_{B-V} derived from L_α measurements in hot stars (cf. Savage & Jenkins 1972).

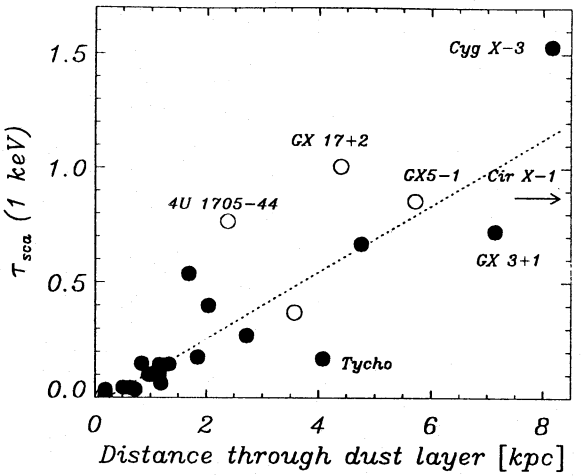

Fig. 5. Optical depth in scattering vs. distance through galactic dust layer. The latter has been calculated according to $dist[kpc] = 0.1 / sin(b^{II})$. Filled circles denote sources for which the visual extinction is known. Sources represented by open circles are not optically identified (apart from Tycho). Only the filled circles have been used for the fit (dotted line). Sources close to that line lie probably outside of the galctic dust layer, sources below that line still within. Sources above the dotted line show an excess in dust column density

3.3. Fractional halo intensity and galactic latitude

Since X-ray halos are produced by scattering off dust grains (which are thought to be confined to the disk of the Galaxy with a typical scale height of $\approx$ 100 pc; cf. Spitzer 1978), one expects a correlation between the halo strength as measured through its fractional intensity and the galactic latitude (except the 'calibration source' PKS 2155-304) of the X-ray source. As is clear from Table 2, all our sources are at low galactic latitude, and we in fact have not been able to find any X-ray halos at b > 20°. In Fig. 4 we plot the derived dust optical depth $\tau_{sca}(1keV)$ vs. galactic latitude; Figure 4 reemphasizes

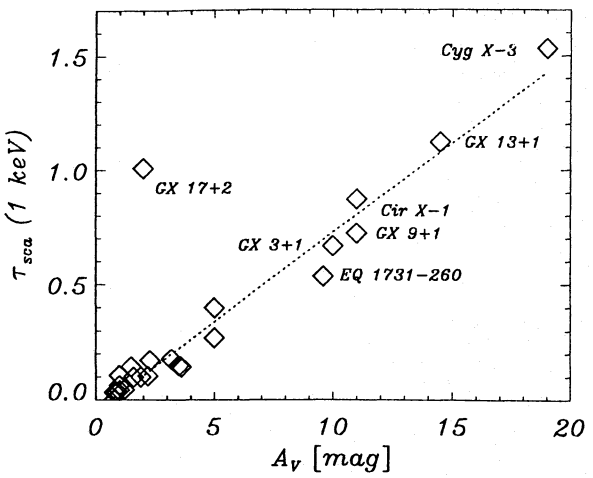

Fig. 6. Effective optical depth in scattering vs. visual extinction for optically identified sources. The optical depth at 1 keV has been calculated according to $\tau_{sca}(1keV) = \tau_{sca} * E^2$ in order to compare halos obtained by different photon energies. The fit to the data (dottet line) yields $\tau = 0.058 \times A_V - 0.013$; GX 17+2 was excluded from the fit

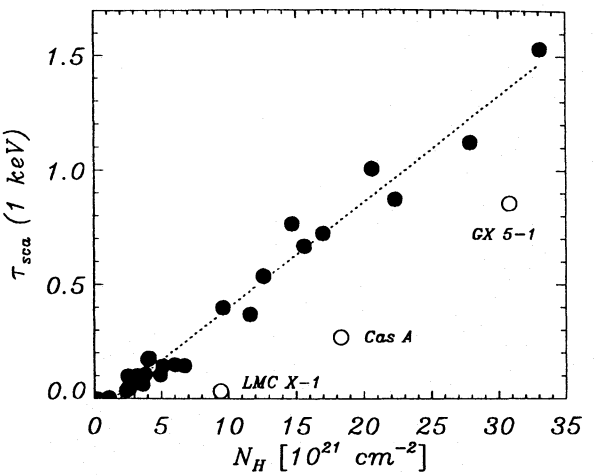

Fig. 7. Optical depth in scattering vs. neutral hydrogen column density. The fit (dotted line) does not contain GX 5-1, Cas A, and LMC X-1

our point that strong X-ray halos are only found in the vicinity of the galactic plane. We can now convert the galactic latitude into an effective distance through the galactic dust layer d_{dl} (calculated from $d_{dl} = 0.1/sin\, b^{II}[kpc]$). In Fig. 5 we plot τ_{sca} vs. d_{dl} (filled dots denote sources with optically known visual extinctions, open dots denote unidentified sources (except for Tycho)); the dotted line represents the best linear fit to the data. Most of the sample sources seem to obey a linear correlation quite well. Sources below the correlation line (Tycho, GX 3+1, and Cir X-1) are interpreted to lie within the galactic dust layer, i.e., their distance is less than the total galactic line of sight. Other sources show an excess in dust scattering which suggests the presence of foreground dust clouds in addition to the average value. All other sources may lie at the edge or even outside the galactic dust layer, for instance in globular clusters.

3.4. Fractional halo intensity and visual extinction

Since X-ray scattering (measured through the derived scattering optical depth τ_{sca}) and optical extinction (measured through A_v) are produced by essentially the same dust grains, a strong correlation should exist between both quantities. For the subsequent analysis, only 24 sources have been used since not all of the sources of our sample are optically identified. In Fig. 6 we plot τ_{sca} vs A_v for these 24 sources. For all sources (except GX 17+2, see above) a strong correlation does indeed exist as expected. The linear regression between τ_{sca} and A_v yields $\tau_{sca} = 0.057 \times A_v + 0.09$. Assuming that the visual extinction is caused by spherical grains with an average radius a_g and column density N_g, we can express A_v as $A_v = 1.086\, N_g\, \pi\, a_g^2\, Q_{ext}$, where Q_{ext} denotes the extinction efficiency at visual wavelengths. Similarly, the scattering optical depth τ_{sca} is related to the scattering efficiency Q_{sca} through $\tau_{sca} = N_g \pi a_g^2 Q_{sca}$, and therefore the proportionality between A_v and Q_{sca} can be attributed to that between Q_{ext} and Q_{sca}. Using the expression

$$Q_{sca} = 0.2\,(\frac{2Z}{M})^2\,(\frac{\rho}{3})^2(\frac{a}{0.1\mu m})^2 \times (\frac{E}{1KeV})^{-2}(\frac{F(E)}{Z})^2 \quad (4)$$

(cf. Mauche & Gorenstein 1986), where Z and M denote atomic charge and mass respective, F(E) the atomic scattering factor, and ρ and a the grain density and size, we find

$$\frac{\tau_{sca}}{A_v} = \frac{0.2}{(1.086\, Q_{ext}}(\frac{2Z}{M})^2\,(\frac{\rho}{3})^2(\frac{a}{0.1\mu m})^2 \times (\frac{E}{1KeV})^{-2}(\frac{F(E)}{Z})^2. \quad (5)$$

Except for the grain size a, none of the parameters entering Eq. (4) varies strongly, and $Q_{ext} \sim 2$; thus the measured ratio $\tau_{sca}/A_v = 0.056 \pm 0.01$ must essentially be due to the effective grain size of those grains responsible for the X-ray scattering. Putting in the measured values we find rather large grain sizes. This, however, is no great surprise since the total scattering optical depth is dominated by the larger particles unless the particle size distribution is extremely steep when going towards the smallest particle sizes.

3.5. Fractional halo intensity and absorption column density

Since the absorption column density N_H and visual extinction A_v (cf. Fig. 3) and X-ray scattering optical depth τ_{sca} and visual extinction A_v (cf. Fig. 6) are correlated, it comes of course as no surprise that absorption column density N_H and X-ray scattering optical depth τ_{sca} are also correlated. This is demonstrated in Fig. 7, where we plot τ_{sca} vs. N_H for **all** our sample sources; three sources, LMC X-1, Cas A, and GX 5-1, plotted with open circles in Fig. 7, fall below the regression line. A linear regression between τ_{sca} and N_H yields $\tau_{sca} = 0.05 * N_H[10^{21} cm^{-2}] - 0.083$. One should, however, bear in mind that N_H as measured through X-ray absorption is mainly determined by the metal abundances in the interstellar

medium, while τ_{sca} is a property of the dust grains. The close correlation between the dust related quantities τ_{sca} and A_v on one hand and the interstellar absorption N_H on the other hand implies that the interstellar medium is solely responsible for the total amount of absorption in all cases but that of GX 5-1. The case of LMC X-1 has already been discussed in Sect. 3.2. As far as Cas A is concerned, we note that it shows too large an interstellar absorption column N_H given its optical extinction **and** fractional halo intensity (cf. Figs. 3 and 7). We consider the possibility that our derived N_H values overestimate actual hydrogen column densities unlikely since they reasonably agree with literature values. This, however, has an interesting consequence: There are no reports on the supernova producing Cas A. This is quite surprising since this supernova must have have been very bright given its low (nominal) A_V. Increasing this would therefore explain why Cas A's supernova was not recognised by optical observers; in this case, however, one has to demand that the dust responsible for extinction and X-ray scattering is very close to the remnant and, therefore, cannot contribute to the scattering and is probably missed also by the extinction measurement. Alternatively, the supernova explosion might have destroyed the dust layer obscuring the supernova event in the first place.

3.6. Energy dependence of scattering

When analysing a halo of a source within different energy bands of its spectrum, the general tendency of $I_{halo} \sim E^{-2}$ is proven. But no further statements about the energy dependency of the scattering cross section, which can provide clues to chemical constituents of the grains, can be made. In order to demonstrate the effect of energy dependence of the halo brightness we have plotted in Fig. 8 for GX 17+2 the derived fractional halo intensity vs. mean photon energy.

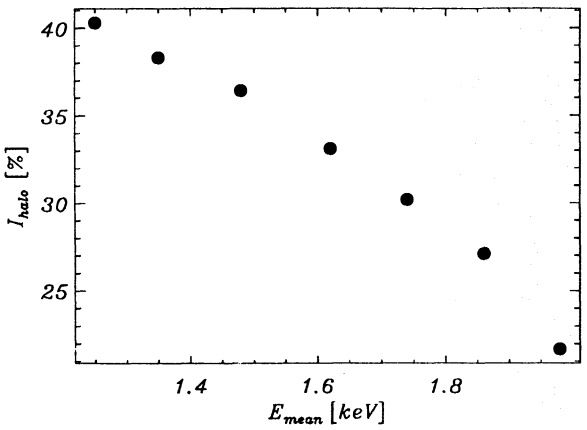

Fig. 8. Relative halo intensity vs. average photon energy for GX 17+2. The pulse height spectrum has been split into individual bands. The photon energies contributing to a band have been weighted by the total scattering cross section

3.7. Is multiple scattering important ?

Mathis & Lee (1991) have pointed out the role of multiple scattering events in the halo formation: Multiple scattering events tend to make the observed halo broader (in comparison to a single scattering halo), while the inner (small-angle scattering) halo is dominated by single scattering. At 1 keV, i.e., an energy where the ROSAT PSPC is particularly sensitive, such higher order scatterings should dominate for $\tau_{sca} > 1.3$ or $N_H > 1.5 \times 10^{22} cm^2$. Suffering from such a high absorption, those sources are observed at only at higher energies thereby reducing the (observed) optical depth. The highest observed optical depth (Cyg X-3) is of the order of 0.5. In our analysis we do not directly use the shape of the halo, but only its fractional intensity. Although our model halos (cf. Eq. 1) do not include multiple scattering, the derived fractional halo intensity should be correct as discussed in Sect. 2.2. At any rate, from the values quoted in Table 3 it is clear that multiple scattering will **not** be relevant for any of the sources of our sample.

3.8. Interstellar gas-to-dust ratio

Since both the dust (N_{dust}) and gas column densities (N_H) are measured through our X-ray analysis, it appears that these measurements also constrain the permissible values of the interstellar gas-to-dust ratio. However, at energies above ~ 0.5 keV, the X-ray absorption is almost exclusively dominated by heavy elements, and consequently the actually measured quantity is only the heavy element concentration along a given line of sight, with the equivalent hydrogen column density being inferred by assuming cosmic abundances in the interstellar medium. The same considerations apply to the scattering process, too: Since interstellar dust grains (presumably) contain relatively little hydrogen (and helium for that matter), most of the electrons responsible for the observed scattering are heavy element electrons. We therefore conclude that both absorption and scattering are dominated by heavy elements, and thus our measurements are not sensitive to the hydrogen abundance and mass.

3.9. Element depletion in the interstellar medium

At X-ray energies absorption only depends on the elemental abundances of the heavy elements but not on their chemical composition. Consequently, the amount of X-ray absorption does not depend on whether the heavy elements preferably exist in the gas-phase or are concentrated in grains (we implicitly assume that individual grains are optically thin). The same does obviously not apply to the scattering process. Only those atoms condensed in dust grains contribute to the scattering, and therefore our measurements should provide information on the amount of heavy element depletion in the interstellar medium.

As a starting point for our discussion we take the observed correlation between τ_{sca} and N_H shown in Fig. 7; in order to obtain an effective optical scattering depth of $\tau_{sca} = 1$, an equivalent hydrogen column density of $N_H = 2.3 \times 10^{22} cm^{-2}$ is required. Using the usual expression for the scattering cross

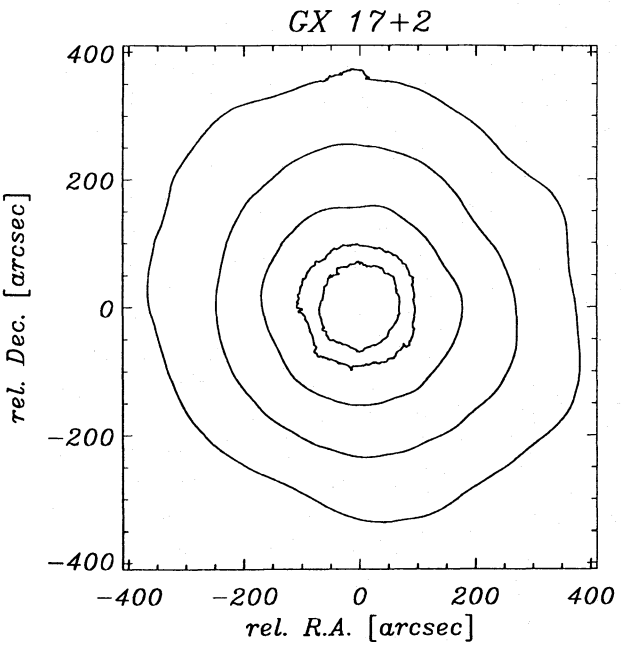

Fig. 9. Surface brightness distribution around GX 17+2. Contour lines correspond to 0.125, 0.25, 0.5, 1, and 2 cts s^{-1} $arcsec^{-2}$. The surface brightness is dominated by the PRF within about 50 arcsec radius

section (cf. Mauche & Gorenstein 1986, Eq. 11) as well as assuming spherical grains, we can express the number of atoms required to form grains producing an optical depth of unity in scattering as:

$$N = \frac{9 \times 10^{18}}{\rho[g\ cm^{-3}]\ a_m[\mu m]} \frac{\sum n_i m_i^2}{\sum n_i m_i \sum n_i F_i(E)^2} \quad (6)$$

with ρ is denoting the mass density, a_m the average grains size radius, n_i the number of atoms of the species i, m_i their atomic weight, and $F_i(E)$ the corresponding atomic scattering factor. As X-ray absorption, X-ray scattering also does not depend on the chemical constitution of the grains but only on the element abundance. Therefore, the atomic scattering factors can be calculated for each atom individually and then summed over all atoms and all species i. From the dust parameters listed in Table 3 one can determine a mean grain radius a = 0.1μm. In Table 4 we have calculated to which extent an individual element can contribute to the scattering optical depth, assuming that it is completely depleted. The contribution depends strongly on the assumed mass density; taking nominal values for condensed matter enables iron (7.9 g cm^{-3}) to produce the total observed scattering almost alone. If all heavy elements and large amounts of oxygen and carbon are depleted (e.g. Morrison & McCammon 1983), grains have to be porous with voids up to about 70%; this agrees well with recent theories (e.g. Greenberg & Hage 1990).

3.10. Clumpiness of interstellar medium

From surveys of the Galaxy in CO and HI emission the interstellar medium is known to be rather clumpy, and a significant fraction of its mass appears to be concentrated in dense clouds. Therefore, one would expect X-ray halos to reflect this clumpiness, too. If most of the dust grains responsible for the production of the dust scattering halo around some source were spatially confined to a few clouds smaller than the halo (typically 10 arcmin, cf. Fig. 10) or and larger than the angular resolution of the *ROSAT* telescope ($\approx$ 25 *arcsec* on axis), one would expect azimuthal asymmetries in halo surface brightness distribution. Our study, however, does not provide any indication for such an inhomogeneous dust distribution neither in longitudinal nor in lateral direction. As an example for this, we present in Fig. 9 a contour plot of the dust scattering halo around GX 17+2. As is clear from Fig. 9, the halo is extremely symmetric with no indication for any deviation from azimuthal symmetry, and appears to be typical for the halos covered by our study. Thus, while keeping in mind the caveat that the dust distribution along the line of sight cannot be determined independently from the grain properties, the most natural way to interpret this finding is to assume that the observed dust scattering halo is in fact an average over many clouds at different distances. Putting it differently, it appears that the scattering centers producing the dust scattering halos are not clumped, rather they seem to be distributed quite uniformly on a Galactic scale. This conclusion is supported by the tight correlation between the optical depth in scattering and the visual extinction (cf. Fig. 6). While the latter quantity is produced on a very small scale and might be affected quite easily by clouds even smaller than the angular resolution of our telescope, dust scattering is a result of an effect on a much larger scale.

4. Conclusions

We have studied diffuse X-ray emission around compact point-like sources and four supernova remnants. The sample studied is complete in the sense that it comprises all galactic sources detected with count rates in excess of 5 cts s^{-1}in the ROSAT all-sky survey as well as sufficient absorption. For 25 sources we find statistically significant excess emission (over that of the central point-like source) which we attribute to the presence of dust scattering halos. Thus, the stronger X-ray sources with a substantial cut-off in their spectrum (i.e., $N_H \geq 2 \times 10^{21} cm^{-2}$) are always surrounded by a dust scattering halo detectable at photon energies of $\approx$ 1 keV.

We have analysed the radial brightness distribution profiles of the halos with a simple analytical model which allows us to determine in particular the fractional halo intensity, the maximum grain size, and the slope of an assumed power law grain size distribution. The derived fractional halo intensities span the range from a few percent to a little over 40 percent for the source Cyg X-3, implying dust scattering optical depths of $\approx$ 0.5 at most. Thus multiple scattering effects are not important for any of our sources.

The X-ray derived dust scattering optical depths correlate well with the also X-ray derived absorption column densities, and the optically derived visual extinctions; further, the derived dust column densities are anti-correlated with galactic latitude

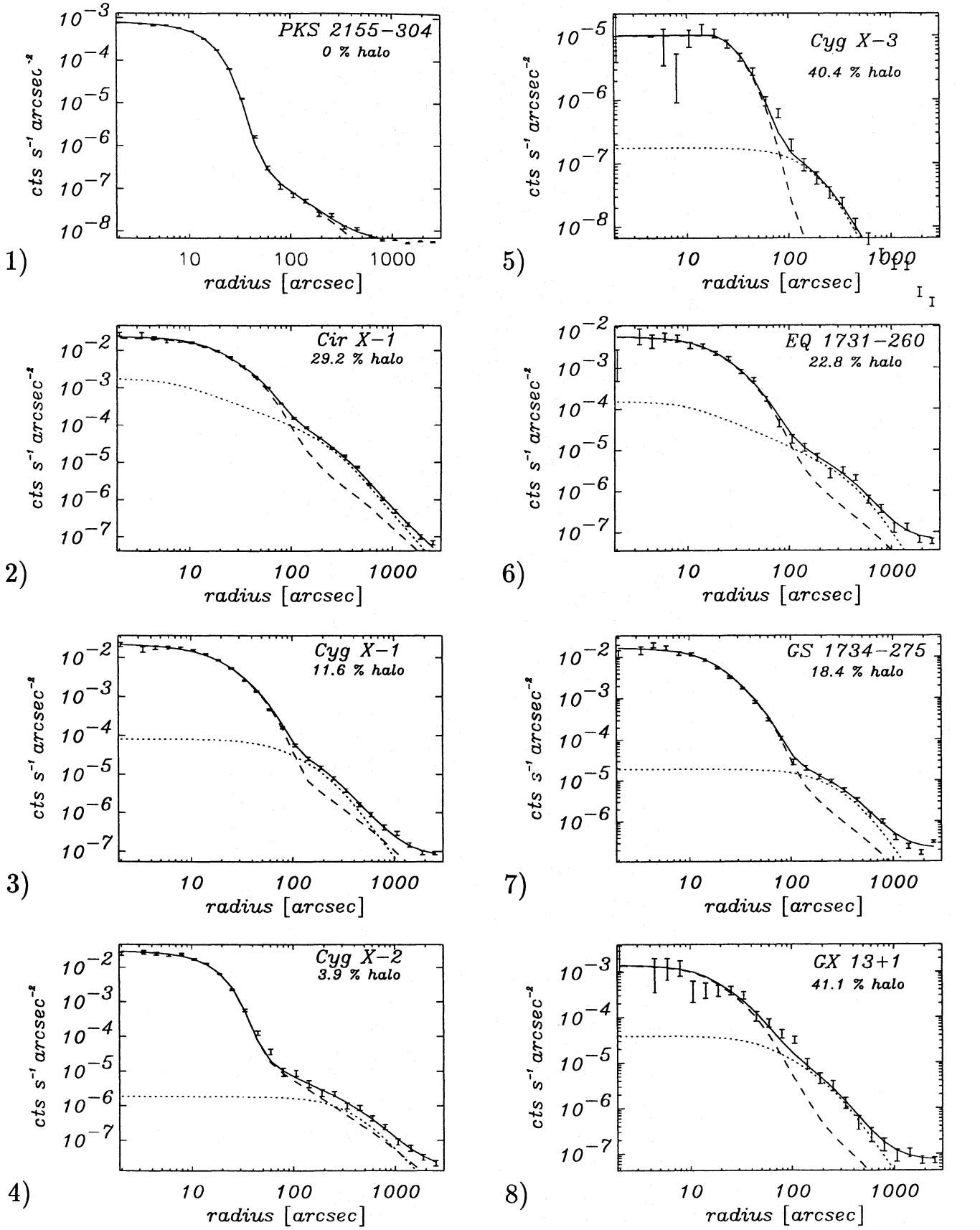

Fig. 10. Surface brightness distributions for 29 different sources. Measurements are represented by their 1σ error bars. The fits to the data (solid line) comprise the point response function (PRF, dashed line) the background and the halo model (dotted line). Pointed observations are recognized by their relatively narrow PRF (1, 9, 12, 13, 14, 21, 22 and 24. For the fit to the data of extended sources (26 – 29), but also for Cyg X-3 (5), the PRF was broadened by a simple boxprofile. The relative halo brightness is given with each source

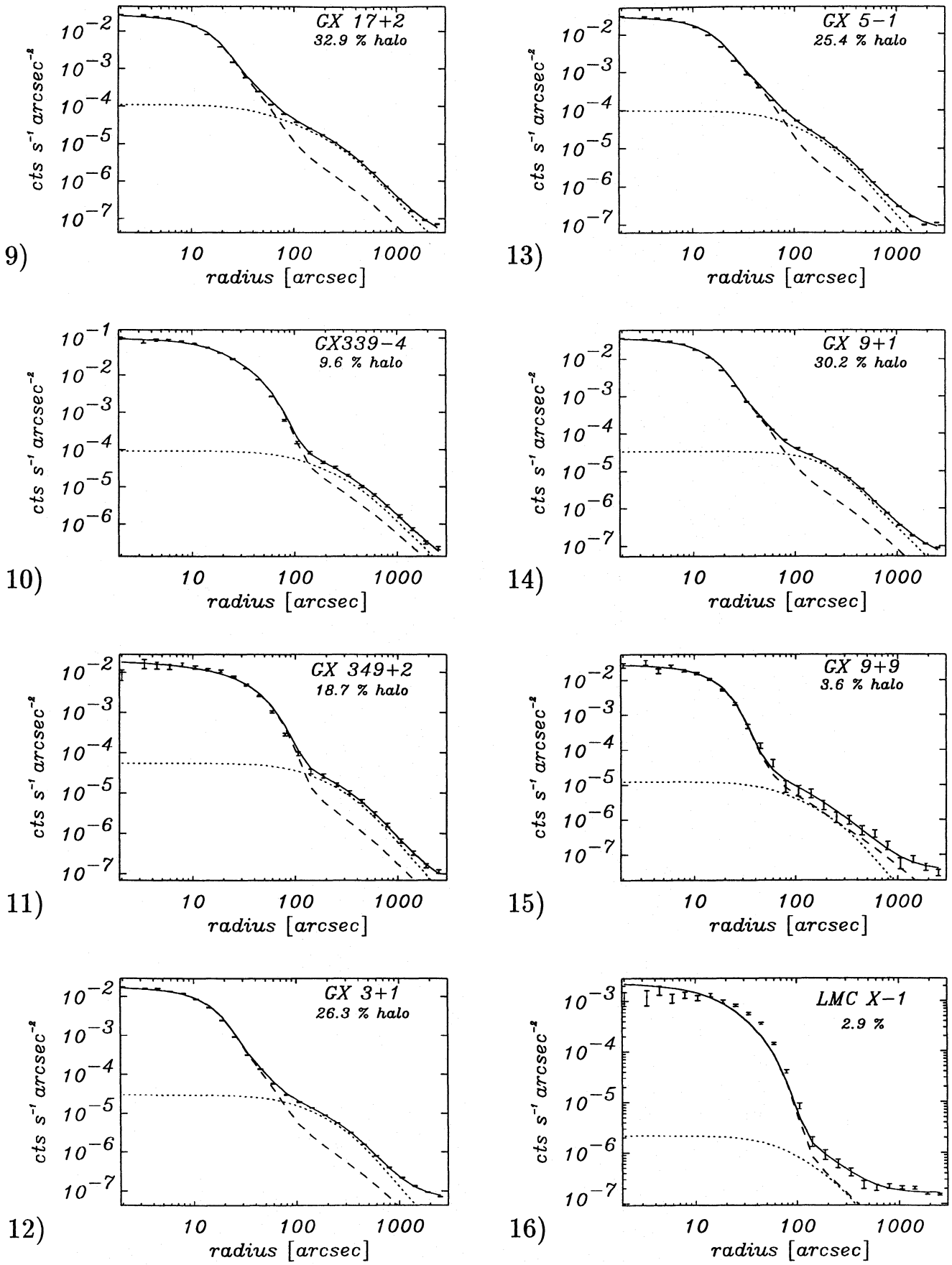

Fig. 10. (continued)

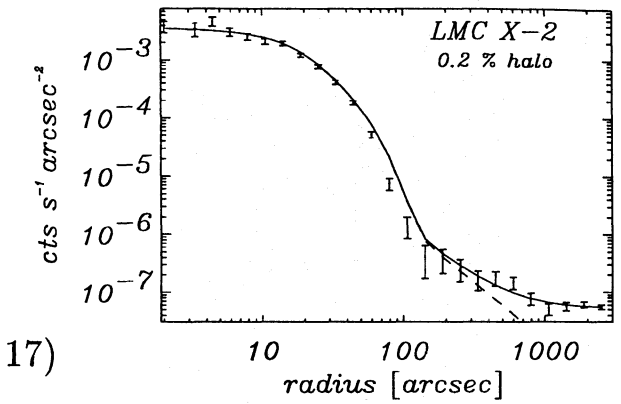

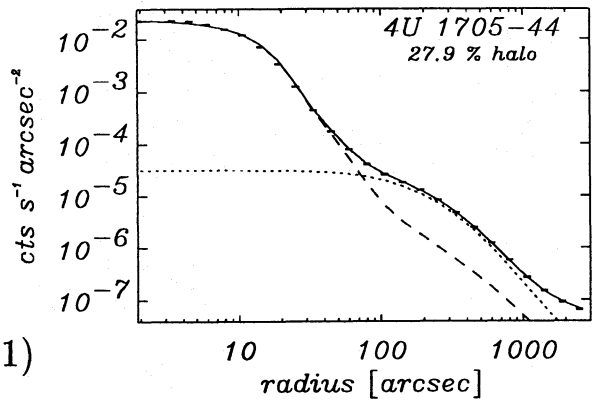

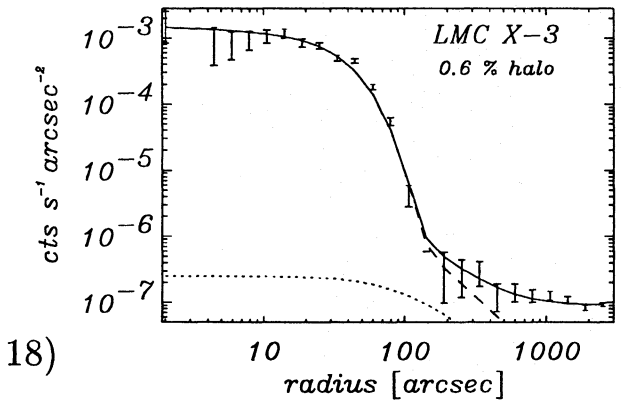

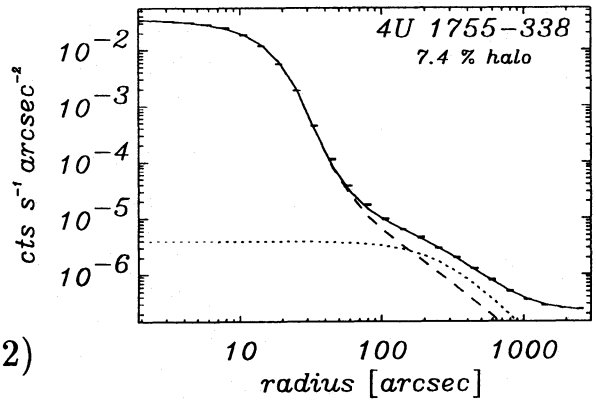

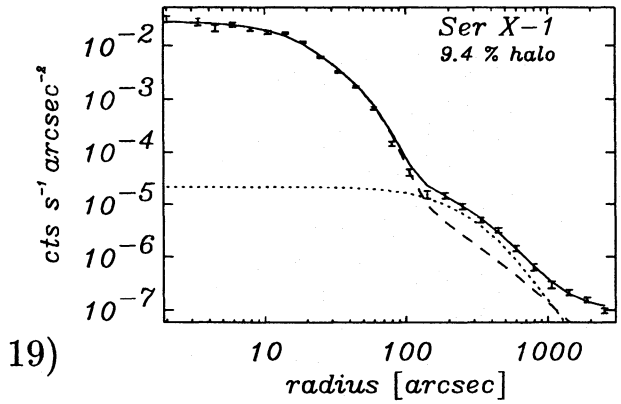

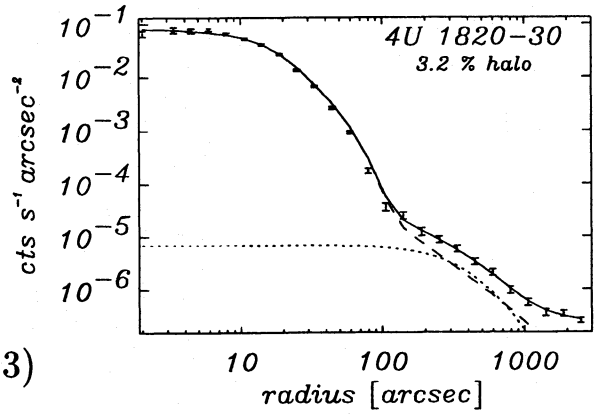

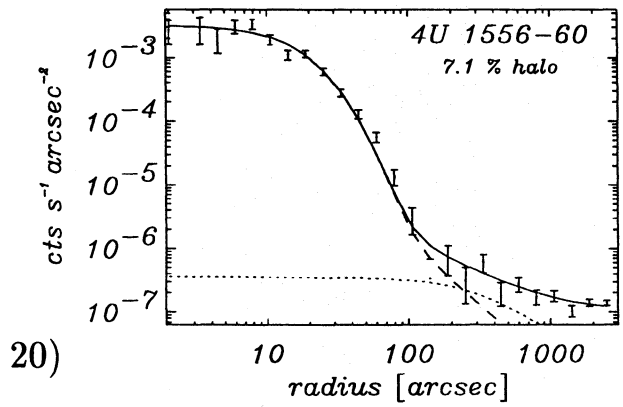

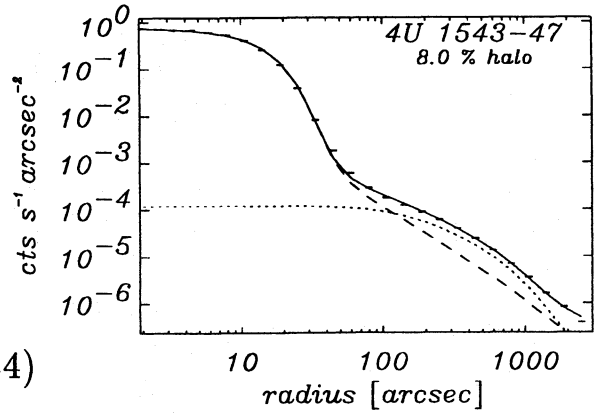

Fig. 10. (continued)

Table 4. List of elements with their atomic scattering factors at 1 keV (Henke 1991), their column density using cosmic abundances (Morrison and McCammon 1983) and $N_H = 2.3 \times 10^{22} cm^{-2}$, the atomic weight and the mass density. The last column contains the contribution to an unity optical scattering depth assuming that all atoms are solely in grains.

Element	$F(E)^2$	N [cm^{-2}]	m	ρ [g cm^{-3}]	contr.
C	40	$1.0\ 10^{19}$	12	2.3	83%
N	55	$2.1\ 10^{18}$	14	1.	9%
O	70	$1.7\ 10^{19}$	16	1.	74%
Mg	102	$9.0\ 10^{17}$	24	1.7	8%
Si	167	$8.5\ 10^{17}$	28	2.3	13%
S	240	$4.4\ 10^{17}$	32	1.9	7%
Fe	644	$7.9\ 10^{17}$	56	7.9	77%

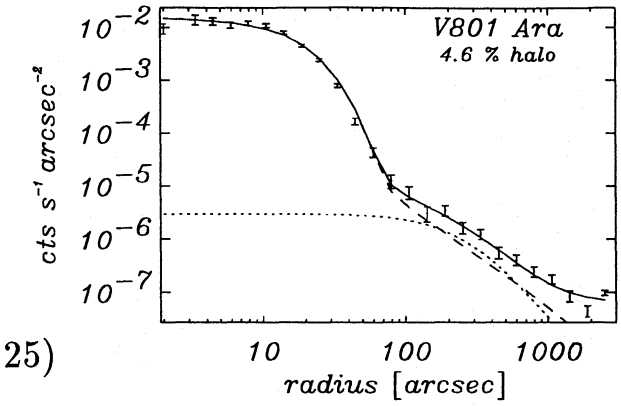

25)

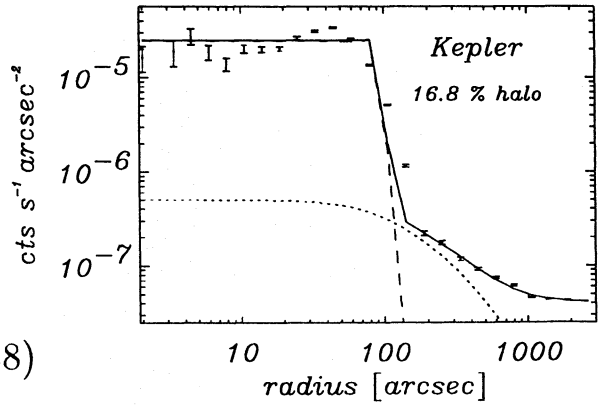

28)

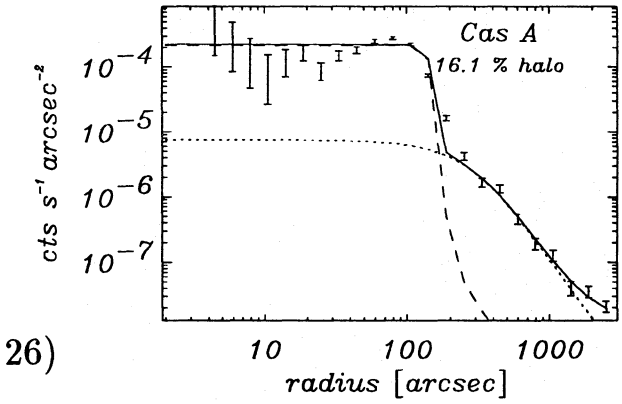

26)

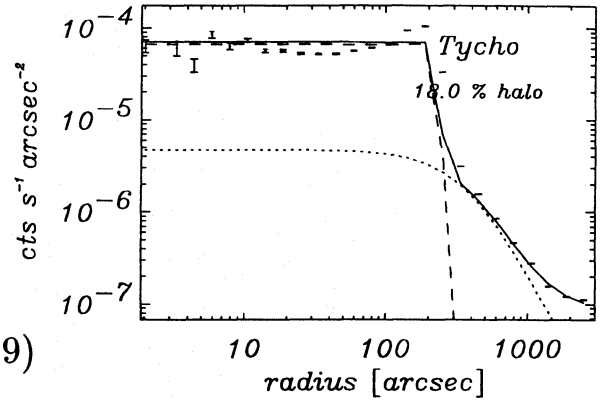

29)

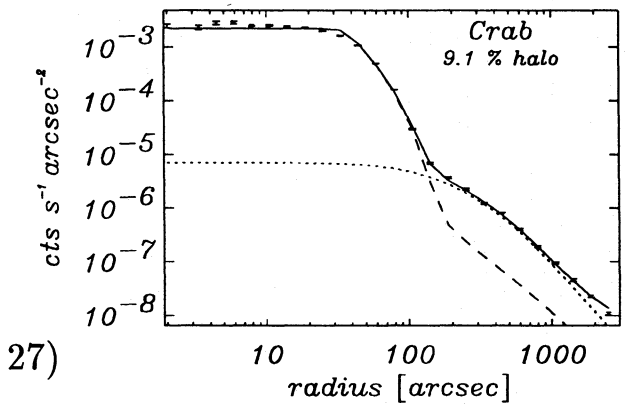

27)

Fig. 10. (continued)

as is the case for optical extinction. Our results therefore suggest a rather uniform gas to dust ratio that is largely independent from the chosen line of sight.

If we leave out the extreme values on both sides, the grain size parameter a_{max}, i.e., the large size cutoff of the assumed power law grain size distribution, spans the range between 0.13 μm and 0.22 μm, but most values cluster near the median value of $a_{max} = 0.18 \mu m$. The derived power law slope indices q span the range between 3.2 and 4.4, with again most values clustered near the median value of $q = 4.0$. Thus our X-ray derived power law distribution indices are generally larger than the canonical value of 3.5 (cf. Mathis et al. 1977). On the other hand, the large-size cutoff a_{max} is generally smaller than the cutoff radius used by Mathis & Wallenhorst (1991). Our results are, however, consistent with the X-ray based results of Bode et al. (1985). In particular, we cannot find any indication for very large porous grains as recently suggested (e.g., Mathis & Whiffen 1989; Greenberg & Hage 1990). Such large grains would produce halos with much stronger cores than observed. Although the core determination is admittedly somewhat uncertain due to the limited instrumental resolution inherent especially to the survey data, the expected brightness distribution from such grains would nevertheless significantly differ from our measurements.

As discussed in detail by Predehl et al. (1991) and Predehl & Klose (1994), some of the dust parameters are complementary: thus, for instance, a dust population of large grains in the vicinity of the Sun is able to produce a halo of similar shape as small grains close to the source. Therefore, from the X-ray data alone, dust grain parameters cannot be properly disentangled from line of sight effects, and higher accuracy results can only be obtained if some parameters are fixed by other means.

Finally, our study does not provide any indication for a significantly clumped dust distribution. Such distributions would lead to asymmetries in longitudinal or in lateral direction which are simply not observed. Rather, the observed halos appear to be azimuthally symmetric to a high degree, from which one concludes that the dust distribution must be rather uniform on a Galactic scale.

Acknowledgements. The ROSAT Mission is supported by Bundesminister für Forschung und Technologie (BMFT) and the Max-Planck-Gesellschaft (MPG). We thank the SASS and EXSAS teams at the MPE for their help in data processing.

References

Bianchi L., Pakull M.W., 1985, A&A 146, 242
Becker R.H., Boldt E.A., Holt S.S., Serlemitsos P.J., White N.E. 1980, ApJ 237, L77
Bode M.F., Priedhorsky W.C., Norwell G.A., Evans A., 1985, ApJ 299, 845
Bradt H.V.D., McClintock J.E., 1983, Ann. Rev. Astron. & Astrophys. 21, 13
Brinkmann W. et al., 1993, submitted to A&A
Catura R.C., 1983, ApJ 275, 645
Chevalier C., 1989, Proc. 23rd ESLAB Symp., ESA SP-296, 341
Cruddace R., Paresce F., Bowyer S., Lampton M., 1974, ApJ 187, 497
Garcia M.R., Grindlay J.E., Bailyn C.D., Pipher J.L., Shure M.A., Woodward C.E., 1992, ApJ 103, 1325
Greenberg J.M., Hage J.I., 1990, ApJ 361, 260
Hamilton A.J.S., Sarazin C.L., Szymkowiak A.E., 1982, ApJ 300,713
Harwitt M., 1988, Astrophysical Concepts, Springer-Verlag, New York
Hasinger G., Langmeier A., Pietsch W., Sztajno M.: 1985, Space Sci Rev. 40, 233
Hasinger G., Boese G., Predehl P., Turner T.J., Yusaf R., Rohrbach G., George I.M. 1993, MPE/OGIP CAL/ROS/93-015, NASA Goddard Space Flight Center
Henke B.L. 1981 in D.T. Attwood and B.L. Henke (eds.) Low Energy X-ray Diagnostics, New York: AIP, 146
Martin P.G., 1970, MNRAS 149, 221
Martin P.G., Sciama D.W., 1970, Astroph. Lett. Comm. 5, 193
Mason K.O., Charles P.A., White N.E., Culhane J.L. Sanford P.W., Strong K.T., 1976, M.N.R.A.S. 177, 513
Mathis J.S., Lee C.-W., 1991, ApJ 376, 490 (ML91)
Mathis J.S., Rumpl W., Nordsieck K.M., 1977, ApJ 217, 425 (MRN)
Mauche C.W., Gorenstein P., 1986, ApJ 302, 371 (MG86)
Mauche C.W., Gorenstein P., 1989, ApJ 336, 843
Mitsuda K., Takeshima T., Kii T., Kawai N., 1990, ApJ 353, 480
Morrison R., McCammon D., 1983, ApJ 270, 119
Neckel Th., Klare G. 1980, A&AS 42, 251
Naylor T., Charles P.A., Longmore A.J., 1992, M.N.R.A.S. 252, 203
Overbeck J.W., 1965, ApJ 141, 864
Penninx W., Augusteijn T. 1991, A&A 246, L81
Pfeffermann E., Briel U.G., Hippmann H., Kettenring G., Metzner G., Predehl P., Reger G., Stephan K.-H. 1987, MPE print **81**
Predehl P., Bräuninger H., Burkert W., Schmitt J.H.H.M, 1991, A&A 246, L40
Predehl P., Schmitt J.H.M.M., Snowden S.L., Trümper J., 1992, Science 257, 935
Predehl, P., Klose S., 1994, submitted to A&A
Rolf D.P., 1983, Nature 302, 46
Schulz N.S., Hasinger G., Trümper J., 1989, Astron. Astrophys. 225, 48
Trümper J., 1983, Adv. Space Res. 2, 241
White N.E., Stella L., and Parmar A.N., 1988, Astrophys. J. 324, 363
Van Paradijs J., 1991, in J. Ventura and D. Pines (eds.) Neutron Stars: Theory and Observation, 245, Kluwer Dordrecht
Voges W., 1992, ESA ISY-3, 9.

This article was processed by the author using Springer-Verlag LaTeX A&A style file version 3.